

# Software Phantom with Realistic Speckle Modeling for Validation of Image Analysis Methods in Echocardiography

Yuen Law<sup>a</sup>, Daniel Tenbrinck<sup>b</sup>, Xiaoyi Jiang<sup>b</sup> and Torsten Kuhlen<sup>a</sup>

<sup>a</sup>Virtual Reality Group, RWTH Aachen University, Aachen, Germany;

<sup>b</sup>Dept. of Mathematics and Computer Science, University of Münster, Münster, Germany

## ABSTRACT

Computer-assisted processing and interpretation of medical ultrasound images is one of the most challenging tasks within image analysis. Physical phenomena in ultrasonographic images, e.g., the characteristic speckle noise and shadowing effects, make the majority of standard methods from image analysis non optimal. Furthermore, validation of adapted computer vision methods proves to be difficult due to missing ground truth information. Until today, there is no widely accepted software phantom in the community and existing software phantoms are not flexible enough to support the use of specific speckle models for different tissue types, e.g., muscle and fat tissue. In this work we propose an anatomical software phantom with a realistic speckle pattern simulation to fill this gap and provide a flexible tool for validation purposes in medical ultrasound image analysis. We discuss the generation of speckle patterns and perform statistical analysis of the simulated textures to obtain quantitative measures of the realism and accuracy regarding the resulting textures.

**Keywords:** Software Phantom, Virtual Organs, Validation, Medical Ultrasound Imaging, Echocardiography, Speckle Noise

## 1. INTRODUCTION

Ultrasound (US) imaging is one of the most challenging modalities for medical image analysis. Due to its underlying physical principles, a variety of perturbations affect the generated images. One of the most significant effects is the inherent physical noise, which leads to grainy textures in the imaged tissue. This so-called *speckle noise* is characteristic for US data and plays an important role, e.g., in tissue classification.<sup>10,16</sup>

In ultrasound image analysis, the current focus of research has moved to appropriate mathematical modeling of speckle and other physical effects.<sup>1,14,17,18</sup> All these methods share the problem of validating the proposed algorithms for automated processing and interpretation of medical US images, which is difficult for real data due to missing ground truth information. To overcome this fundamental problem of validation some authors test their methods on synthetic data generated with the help of software phantoms.<sup>1,17</sup> The main advantage of software phantoms is that *ground truth information* for the validation of image analysis methods is inherently given by the defined data set. However, existing software phantoms either prove to be inflexible for evaluation purposes due to tremendous computational effort,<sup>4</sup> or show a lack of realism caused by simplifying assumptions used for the simulation of the physical principle of ultrasound.<sup>12,21</sup> For this reason, we propose an anatomical ultrasound software phantom which offers a trade-off between realism and flexibility and enables its users to generate physically correct US images for the validation of image analysis methods. Furthermore, we pay special attention to the simulation time and achieve interactivity to further improve the user experience, while allowing to dynamically change properties and parameters during the simulation.

## 2. RELATED WORK

Realistic simulation of ultrasound data is difficult, due to the complexity of the underlying physical principles and their adequate approximation. This task has been investigated before and hence several proposed solutions for ultrasound simulation exist in the literature. These can either be separated with respect to their specific focus (accuracy, real-time interaction, realism), by the artifacts they aim to simulate (structural artifacts, speckle noise) or by the simulation approach they are based on (generative or interpolative). These different aspects make it difficult to compare different algorithms and their respective simulation results qualitatively and quantitatively to one another.

To underline this observation, we present a sample of the diversity of existing approaches by discussing their respective advantages and shortcomings in the following. The most straightforward approach to simulate US images is to solve the underlying *wave equation* numerically for a given geometry and specified conditions, e.g., the transducer geometry.<sup>4,6</sup> All interactions between the US wave and soft tissue are simulated accurately and thus very realistic results are obtained. The disadvantage of this approach is that, due to the computational complexity, generating a single image can take up to several hours, which is rather impractical in many cases. The authors in Ref. 6 present an alternative approach that models wave propagation using the *Westervelt equation*. Additionally, the image generation pipeline, beginning with the pulse transmission, is also simulated to achieve high realism. By solving the respective partial differential equations on the GPU, they are able to reduce simulation time for a single image to less than 80 minutes. In Ref. 12 the simulation is focused on the generation of a realistic *speckle noise* pattern. The geometry of the ultrasonic scan is taken into account to additionally simulate the effects of axial and lateral resolution. However, acoustic shadowing and absorption are not simulated which leads to rather unrealistic images. Nevertheless, this phantom has recently been used for validation purposes.<sup>18</sup> The authors in Ref. 20 use a *geometrical acoustics model* and simulate reflection and transmission of ultrasound rays using acoustic impedance information obtained from CT scans.

We extended the latter approach for the purpose of medical personnel training.<sup>7</sup> By approximating the wave equation with rays, simulation of most of the ultrasonic wave's interaction with tissue is possible, i.e., reflection and transmission, acoustic shadowing, and reverberation. Furthermore, the correct modeling of the US beam enables the simulation of the effects of lateral, elevational, and axial resolution, leading to comparably realistic results. In related areas of research, e.g., ultrasonic tissue characterization, speckle noise has been studied by various authors from a physical point of view, but to the best of our knowledge, their observations have not been used yet in US image simulation to generate realistic speckle noise.

Although all previously discussed works aim for realistic US imaging simulation there is still no widely accepted software phantom for the *validation* of image analysis methods today. This motivates us to propose an anatomical software phantom with realistic speckle noise which provides a flexible simulation tool for validation purposes in medical ultrasound image analysis.

### 3. METHODS

#### 3.1 Physical Noise Models

When coherent light, e.g., a laser beam, encounters tiny particles smaller than the wavelength in a medium, it gets scattered in different directions. Such reflected wavelets arrive at the observation point at different times causing constructive or destructive interferences. The resulting pattern is called *speckle noise* and was first observed and studied with the invention of lasers. Speckle is not an exclusive phenomenon of laser and can be found in other forms of coherent imaging, including ultrasound.

Since scattering particles are often randomly distributed in the medium, speckle noise generation can be treated as a random walk in the complex plane as proposed by several authors.<sup>2,3,12</sup> The models used here assume that there exist a number of scatterers within a so-called *resolution cell*. This cell is the minimum unit of detail that can be resolved by the transducers, this means that objects that share the same cell will be seen as one. The amplitude  $A$  of the detected wave for a single resolution cell is the sum of all the contributions of the reflected wavelets, i.e., the phasors. This can be expressed by:

$$A = \frac{1}{\sqrt{n_t}} \sum_{k=1}^{n_t} |a_k| e^{j\phi_k}, \quad (1)$$

where  $n_t$  is the number of particles in the corresponding cell, and  $a_k$  and  $\phi_k$  are amplitude and phase of the  $k$ th phasor, respectively. For each resolution cell, there exist a number of scatterers with random properties that reflect the ray. These properties, e.g., size, density, and phase, differ between various models in the literature and each model uses a specific probability density function for these random properties. We chose and evaluated three different approaches which are closely related to the general backscattering model in (1), i.e., the ones presented by Insana and Hall,<sup>5</sup> Eltoft,<sup>2</sup> and Narayanan et al.<sup>9</sup>

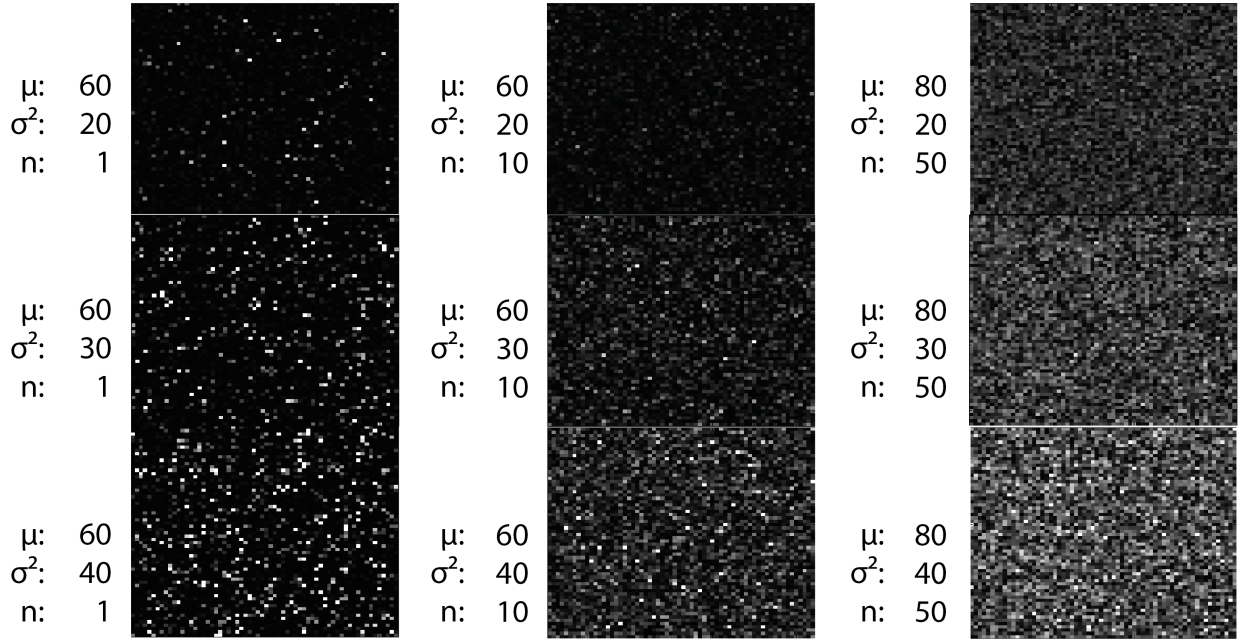


Figure 1. Noise textures generated with the Insana and Hall model using different parameters.

In the following we discuss the details for each of these backscattering models. For clarity, note that we change from the calculation of amplitude  $A$  to the backscattered energy or intensity  $\sigma$ , following that intensity and amplitude differ only by a scaling constant.<sup>3</sup>

### 3.1.1 Insana and Hall model

The model presented by Insana and Hall<sup>5</sup> describes the backscattered energy  $\sigma$  from a single resolution cell by:

$$\sigma = I_i C f^4 \gamma_0 \sum_{k=1}^{n_t} \left[ D_k^6 \frac{n_k}{n_t} F(f, D_k) \right], \quad (2)$$

where  $I_i$  is the incoming intensity and  $C$  is a constant equal to  $\pi^4/36c^4$  with  $c$  being the speed of sound in the medium. Furthermore,  $f$  denotes the simulated ultrasound frequency,  $n_t$  is the total number of scatterers, and  $n_k$  is the number of scatterers with diameter  $D_k$ . Furthermore,  $F$  is the backscattered energy from a single particle given by:

$$F(f, D) = \left( j_0 \left( \frac{2\pi f D}{c} \right) \right)^2, \quad (3)$$

where  $j_0$  is the spherical Bessel function of the first kind and zeroth order. Finally,  $\gamma_0$  is the scattering strength given by the medium and scatterer impedances  $Z_1$  and  $Z_2$ , respectively, i.e.,

$$\gamma_0 = 4 \left( \frac{Z_1 - Z_2}{Z_1} \right)^2. \quad (4)$$

This model assumes a uniform distribution of the scatterers throughout the medium. Hence, it is sufficient to consider only the amount of scatterers disregarding the exact placement and alignment. For the model the number of scatterers  $n_t$  is realized via a Poisson distribution. The diameters of these scatterers are assumed to be normally distributed. Thus, the only free parameters are the expected number of particles per resolution cell and the mean and variance for the diameters of the particles.

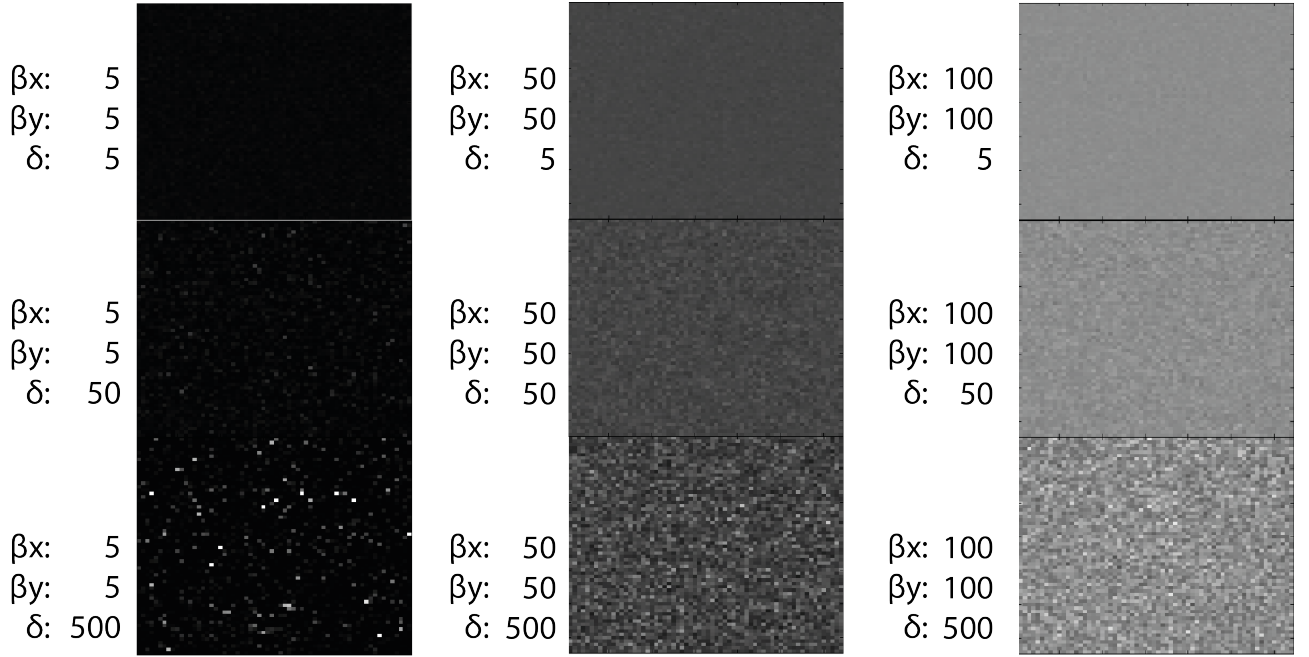


Figure 2. Noise textures generated with the Eltoft model using different parameter settings.

Figure 1 shows different textures generated using this model for different parameter settings. It can be observed how the total number of scatterers  $n_t$  changes the density of the noise, while the variance affects the contrast.

### 3.1.2 Eltoft

The model presented by Eltoft<sup>2</sup> is based on Brownian motion and describes the backscattered energy  $\sigma$  by

$$\sigma = A + \sum_{k=1}^{n_t} a_k e^{j\phi_k} = \sum_{k=1}^{n_t} \beta_x + j\beta_y + a_k e^{j\phi_k} = X + jY, \quad (5)$$

where  $n$  is the number of scatterers in the cell and  $a_k$  and  $\phi_k$  are the amplitude and phases of the  $k$ th scatterer, respectively. As can be seen, the  $X$  and  $Y$  components can be treated as two Brownian motions with respective drifts  $\beta_x$  and  $\beta_y$ . Furthermore, let  $Z$  be a fixed random variable, then  $X$  and  $Y$  can be expressed as:

$$X = \beta_x Z + \sqrt{Z} N_x, \quad Y = \beta_y Z + \sqrt{Z} N_y,$$

where  $N_x$  and  $N_y$  are standard normal distributed random variables. Following Ref. 2, we also assume that  $Z$  follows approximately an inverse Gaussian distribution with mean  $\delta$  and variance  $\gamma$ , expressed by:

$$\gamma = \sqrt{\beta_x^2 + \beta_y^2}. \quad (6)$$

The only free parameters for this model are the two values for the Brownian motion drifts  $\beta_x$  and  $\beta_y$ , and the values for  $\delta$  and  $\alpha$  used for the distribution of  $Z$ . Apart from some examples, Ref. 2 does not give much further insight about the values that these parameters should take or how they influence the pdf, therefore, we have chosen and tested arbitrary values.

Figure 2 shows noise textures generated with different parameter settings. In comparison to the previous model, the Eltoft model produces more homogeneous textures. Increasing the value of  $\delta$  increases the contrast of the noise, while the  $\beta$  values change the overall brightness.

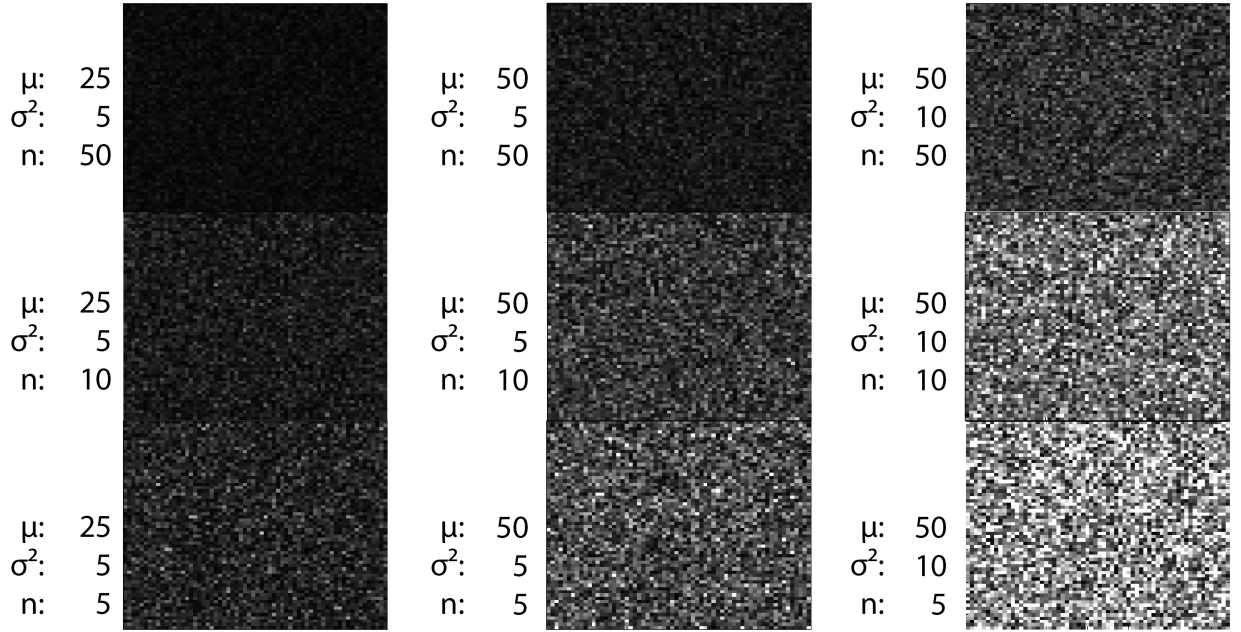


Figure 3. Noise textures generated with the Narayanan model using different parameter settings.

### 3.1.3 Narayanan

For the Narayanan model in Ref. 9 the received energy is also described as a sum of echoes from the scatterers in the resolution cell. In this case, amplitude and position are varied from scatterer to scatterer to obtain the total energy, which is given by:

$$\sigma = \sum_{k=1}^{n_t} \alpha_k P\left(\frac{2x_k}{c}\right), \quad (7)$$

where  $n_t$  is the number of scatterers in the resolution cell.  $\alpha_k$  and  $x_k$  are the amplitude and distance from the transducer of the  $k$ th scatterer, respectively, and  $c$  is the speed of sound. Finally,  $P(t)$  is the transmitted pulse given by:

$$P(t) = -t e^{-4\beta^2 t^2} \sin(2\pi f_0 t), \quad (8)$$

where  $f_0$  is the simulated center frequency and  $\beta$  the frequency bandwidth of the ultrasonic pulse. In Ref. 9, these values were set to  $3.5MHz$  and  $0.8MHz$  respectively. As our simulation allows the use of different values for  $f_0$ , we keep the same ratio and set  $\beta$  accordingly.

As in the case of Insana and Hall, scatterers are assumed to be uniformly distributed across the medium and here the number of scatterers  $n_t$  is also determined by a Poisson distribution. Additionally, the distance  $x_k$  follows a uniform distribution. Since the backscattered energy of each resolution cell is calculated independently from each other, i.e., no multi-scattering is taken into consideration, relative positions of the scatterers within each cell are used. Thus,  $x_k$  takes values between 0 and 1. The amplitudes  $a_k$  are assumed to have a Gamma distribution in accordance with the models presented in Ref. 9 and Ref. 16.

Figure 3 shows different noise textures generated with the Narayanan model using different parameter settings for the mean and variance of the Gamma distribution that defines the amplitudes of the scatterers and the average number of scatterers in each resolution cell. It is clear here, that the total number of scatterers  $n_t$ , as well as the amplitude  $a_k$ , determined by the values  $\mu$  and  $\sigma^2$ , have a direct influence on the density and intensity of the generated noise textures.

### 3.2 Speckle Texture Simulation

Medical ultrasound image simulation approaches usually apply only one speckle noise model throughout the entire image, ignoring the properties of individual tissue types. This is commonly realized by one of the following three techniques: i) generating noise as random values from parametric distribution functions such as the Rayleigh distribution<sup>13</sup> and applying them pixel-wise in a post-processing step; ii) using speckle textures taken from real ultrasound images;<sup>21</sup> or iii) sampling a field of random scatterers.<sup>7,12</sup> The last option offers most flexibility for simulating US images, since it does not only allow using acoustic properties of the simulated underlying tissue during the generation of scatterers, but also allows to adjust parameters such as their respective *size*, *density*, and *alignment* as discussed above.

To integrate the physical backscattering models in Section 3.1 into our simulation pipeline, we use the following methodology. The three described backscattering models are used to generate three dimensional textures which can be sampled by a raytracing approach during simulation as will be described in Section 3.3. Each *voxel* of the 3D texture represents one resolution cell. The sampling takes place on a regular grid as the rays travel through the scene. The sampled values are combined with the values of the resulting reflection or absorption at the corresponding position, whenever necessary. The 3D noise texture sampling in combination with the ray-tracing process creates the desired speckle pattern. Figure 4(a) shows different simulated speckle textures using these three models with different parameter settings.

### 3.3 Geometrical Acoustics-based Ultrasound Simulation

In our previous work,<sup>7</sup> we proposed an interactive and visually convincing US simulation for *medical training purposes*. It includes simulation of physical effects such as shadowing and reverberation. Our simulation uses a *geometrical acoustics approach*<sup>19</sup> to approximate the wave-tissue interaction with energy-transporting rays that can be reflected, refracted, absorbed or transmitted according to tissue properties. A virtual ultrasound probe (VUSP) composed of an array of virtual transducers is modeled to determine the origin and direction of the rays; multiple rays are created for each transducer in the VUSP. During a real US image acquisition, the transducers are activated in sequence to sweep the area of interest. The intensity of the received echoes and time between sent pulses and echoes is used to create a 2D B-mode image. This is emulated by the use of virtual transducers that work independently in the scene, sending rays to sample it. As the rays travel through the virtual anatomy, samples of the tissue, scatterer information and acoustic intensity are taken according to the distance and direction of each ray to determine its propagating behavior. The information of all rays is finally combined to create the simulated image. For technical details we refer to Ref. 7.

The simulation process incorporates a parameterizable model of the ultrasonic beam and virtual probe. The acoustic pressure field of the focused ultrasonic beam is pre-calculated and stored as a 3D texture, which is then used to map the energy of the traveling rays. The axial, lateral and elevational resolutions of the transducers in the VUSP are also taken into account to generate the simulated images. The VUSP and the beam profile are parameterized and can be changed to model different US devices with, for example, different frequencies and geometries. Figure 4(c) shows a simulated 2D US B-mode image of the heart phantom in an apical four-chamber view with different speckle textures for muscle, blood, heart and septum using the Insana backscattering model.<sup>5</sup> Note that the simulated acoustic shadowing is caused by the lung that obscures part of the left ventricle. Another realistic detail is given by the highly reflective muscle tissue in the septum of the left ventricle.

### 3.4 Anatomically Correct Heart Geometry

The 4D extended cardiac-torso (XCAT) software phantom<sup>15</sup> is widely used for validating medical image analysis methods. It is based on segmentations from the Visible Human project as well as tagged MRI and gated CT data and provides detailed whole-body voxel data. Furthermore, respiratory and cardiac motion can be simulated. Thus, even ground-truth *motion information* is available from the phantom, which enables, e.g., evaluation of motion estimation methods. The XCAT phantom can be used as anatomically correct geometry to various simulations, e.g., PET, SPECT, or CT data. To the best of our knowledge, it has not yet been used for medical ultrasound imaging. Figure 4(b) shows an enhanced geometry of a human heart from the XCAT phantom. Distinct values have been assigned to each tissue type, e.g., the myocardium, lungs, and ribs. This segmentation is used as input for the simulation pipeline described in Section 3.3 and can be used to select realistic parameter settings.

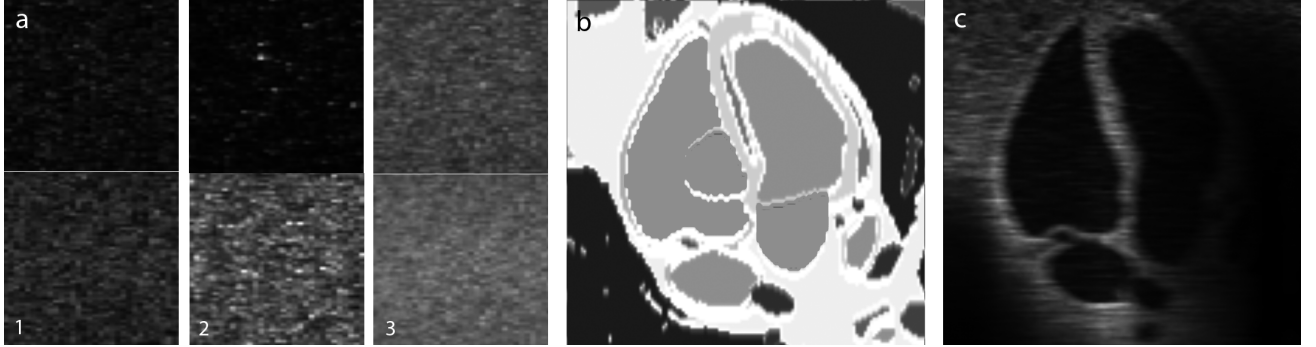


Figure 4. a) Simulated speckle textures for different parameter settings using the backscattering models proposed by: Insana and Hall (1), Eltoft (2), and Narayanan et al. (3). b) Example slice of the heart geometry taken from the XCAT phantom. c) Corresponding US image simulation using the Insana model.

Table 1. Values of  $p$  for the KS test to compare generated speckle before (Model) and after raytracing (Simulation) to the Nakagami distribution. Values in bold face indicate that the *null hypothesis* is rejected.

|            | Insana |        |                 | Eltoft          |        |        | Narayanan |        |               |
|------------|--------|--------|-----------------|-----------------|--------|--------|-----------|--------|---------------|
|            | Set 1  | Set 2  | Set 3           | Set 1           | Set 2  | Set 3  | Set 1     | Set 2  | Set 3         |
| Simulation | 0.1086 | 1.0    | 1.0             | <b>0.0012</b>   | 0.9995 | 0.9883 | 1.0       | 0.8284 | 0.8284        |
| Model      | 0.0694 | 0.4010 | < <b>0.0001</b> | < <b>0.0001</b> | 0.1342 | 0.9970 | 1.0       | 0.6858 | <b>0.0430</b> |

## 4. RESULTS

As described in Section 3.4, by using the XCAT phantom, we obtain *ground truth information* required for validation of image analysis methods and a highly detailed geometry for the simulation. Together with physical noise modeling, 3D beam modeling, and the geometrical acoustics approach to simulate US propagation and interaction with tissue, this enables the generation of *very realistic* US images. Since configuration of all relevant parameters and the different generation stages is possible, we obtain a *flexible* tool that enables the simulation of diverse scenarios with a variety of geometries and US properties.

Although the results of our previous work were rated as convincing by medical experts, the realism of the simulated US images was limited, on the one hand, by the high real-time requirements needed for high interactivity during training sessions, and on the other hand, by the limited choice of noise models used to generate the textures of different tissue types. For the purpose of validating image analysis methods, the real-time constraint is less strict, and hence we are able to incorporate even more realism and flexibility into the simulation by adding more rays for each transducer. Additionally, by supporting parameterizable physical noise models, we can simulate a wider range of speckle textures of the different tissue types.

To quantitatively assess the realism of the used speckle models we performed statistical experiments, which are described in the following. First, for each model and set of parameters, we created a number of 3D scattering textures under the assumption that the particles are distributed uniformly across the volume. These volumes were sampled using our raytracing algorithm described in Section 3.3 to create a simulated 2D B-mode image. The gray values of pixels were classified into bins to create an image histogram. Subsequently, we performed a Kolmogorov-Smirnov (KS) test to measure how well these fit with the Nakagami distribution, which provides a general model for speckle noise.<sup>11,16</sup> The same models were used to generate 2D B-mode images *directly* (without sampling from our raytracer) using the same parameters as in the sampled case. The same goodness-of-fit tests were applied to these images and we compared the results of both cases against each other.

The results of the experiments confirm that using only the theoretical backscattering models to generate speckle noise is not enough to obtain realistic noise. Consequently, adding speckle to simulated images in a post-processing step with noise filters and ignoring the image formation pipeline is rather suboptimal. This is also partly demonstrated by the results shown in Ref. 12. Figures 5, 6 and 7 exemplarily show the density plot of the gray values of the noise texture created using the three models respectively, with different parameter sets,

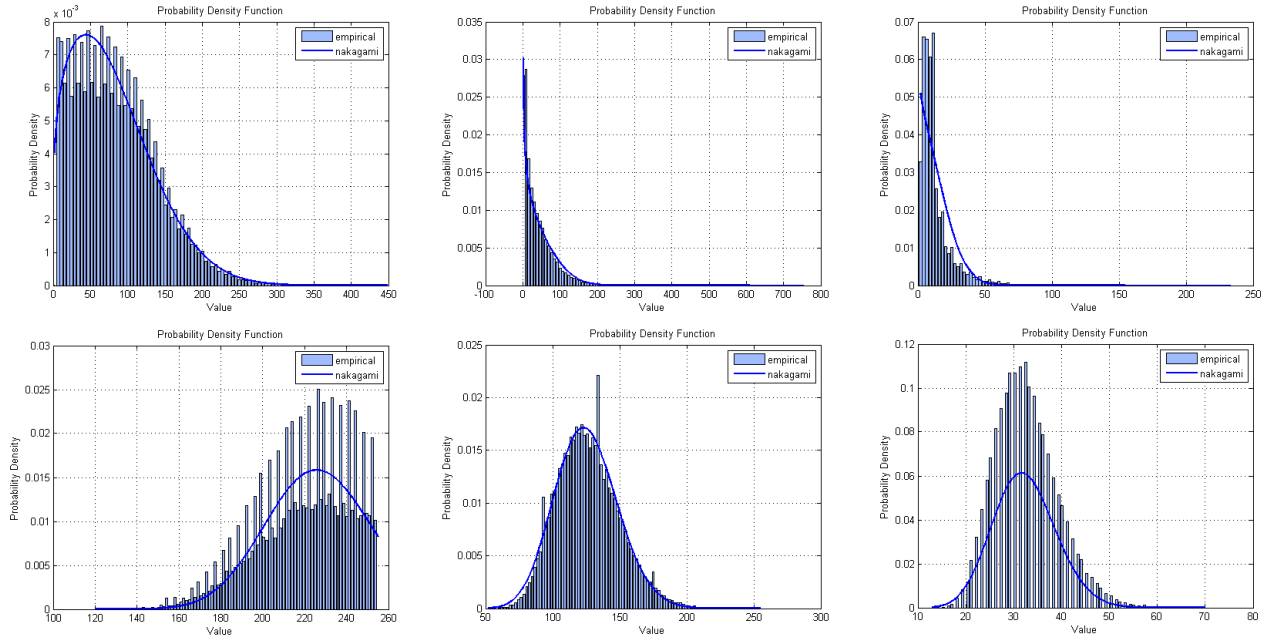


Figure 5. Histograms and Nakagami fits for the Insana model with different parameter sets. Top: *raw* noise models, bot: sampled noise models.

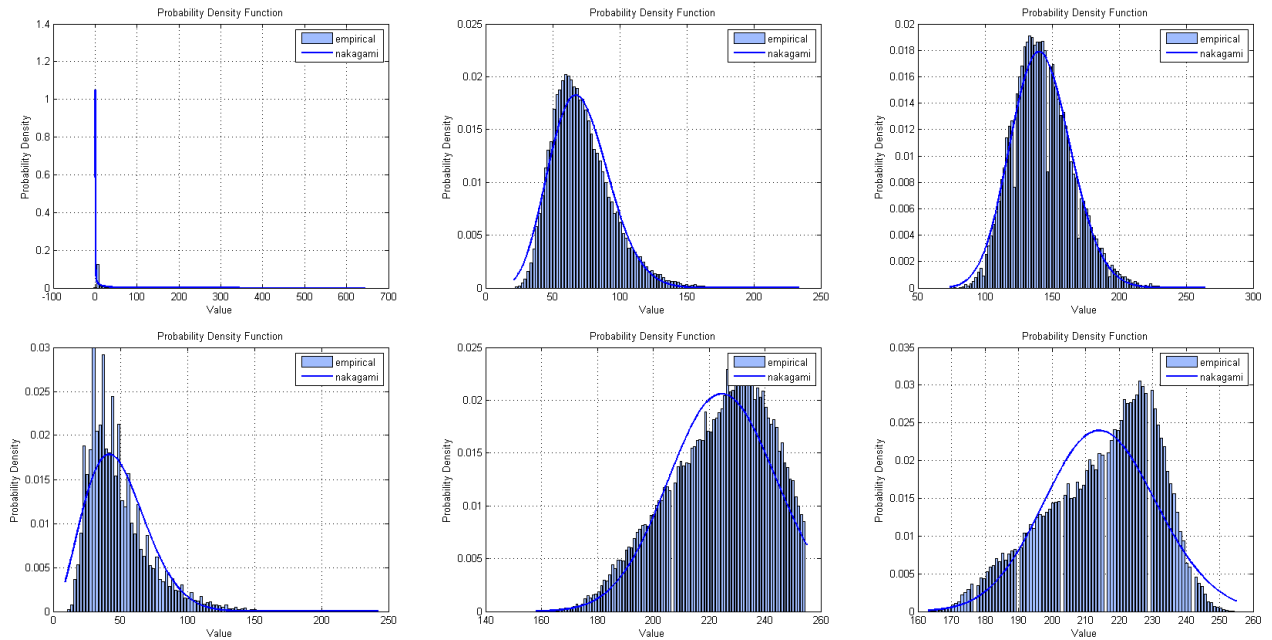


Figure 6. Histograms and Nakagami fits for the Eltoft model with different parameter sets. Top: *raw* noise models, bot: sampled noise models.

before (top) and after (bottom) being sampled by our ray-tracing simulation. Table 1 shows the results of the KS tests for the histograms of the simulated speckle using the plotted data. It can be seen that the *pvalue* for the simulated speckle is higher than that of the *raw* models. The values in bold face indicate the lower *pvalues*, where the *null hypothesis* is rejected. From this, we can conclude that the Nakagami distribution fits the simulated speckle noise better. As can be seen, from a statistical point of view, the combination of the backscattering

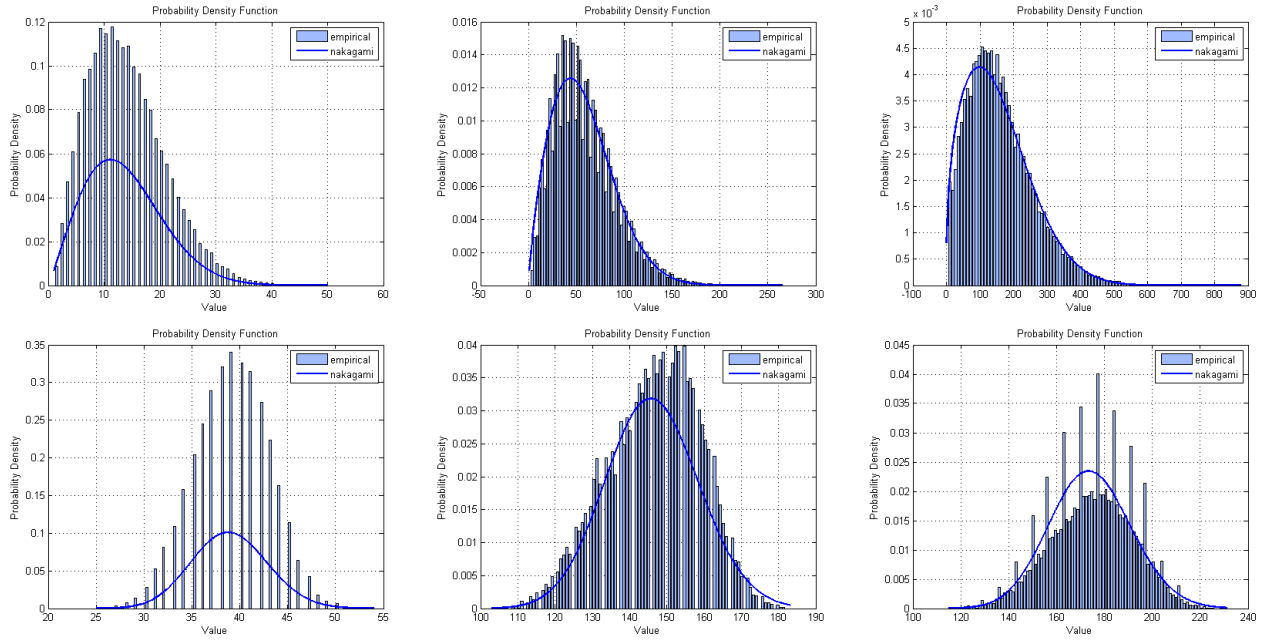


Figure 7. Histograms and Nakagami fits for the Narayanan model with different parameter sets. Top: *raw* noise models, bot: sampled noise models.

model with our simulation pipeline yields highly realistic speckle patterns.

## 5. CONCLUSION

In this work we presented a flexible software phantom that allows simulation of medical ultrasound images incorporating realistic speckle noise models. Three factors contribute to the overall realism of the speckle patterns: i) 3D backscattering fields are created using established physical models; ii) the sampling algorithm uses a realistic focused 3D beam model and iii) for each type of simulated tissue a different backscattering field is created. Furthermore, we presented statistical data to support our claim that the generated speckle is not only visually realistic, but can also be fitted with theoretical models and hence used for validation of image analysis methods. In particular, the resulting speckle noise pattern after simulation can be described by a well-known Nakagami probability density function.

## REFERENCES

- [1] Boukerroui, D.: A Local Rayleigh Model with Spatial Scale Selection for Ultrasound Image Segmentation. In: Proc. of British Machine Vision Conference (BMVC), pp. 84.1–84.12 (2012)
- [2] Eltoft T.: The Rician Inverse Gaussian Distribution: A New Model for Non-Rayleigh Signal Amplitude Statistics. IEEE Transaction on Image Processing. vol. 14, no. 11, pp. 1722-1735. IEEE (2005)
- [3] Goodman, J.W.: Statistical properties of laser speckle patterns. In: Coll. Laser Speckle and Related Phenomena, Springer Berlin Heidelberg, Topics in Applied Physics, vol. 9, pp. 9-75 (1975)
- [4] Jensen, J.A.: Field: A Program for Simulating Ultrasound Systems. In: Proc. of Nordic-Baltic Conf. on Biomedical Imaging (NBC), pp. 351–353 (1996)
- [5] Insana, F, and J Hall.: Parametric Ultrasound Imaging from Backscatter Coefficient Measurements: Image Formation and Interpretation. Ultrasonic Imaging, vol. 12, Issue 4, pp. 245-267. (1990)
- [6] Karamalis, A., Wein, W., Navab, N.: Fast Ultrasound Image Simulation Using the Westervelt Equation. In: Proc. of Int. Conf. on Medical Image Computing and Computer Assisted Intervention (MICCAI), pp. 243–250 (2010)

- [7] Law, C.Y., Knott, T., Hentschel, B., Kuhlen, T.: Geometrical-Acoustics-based Ultrasound Image Simulation. In: Proc. of Eurographics Workshop on Visual Computing for Biomedicine (VCBM), pp. 25–32 (2012)
- [8] Lecellier, F., Jehan-Besson, S., Fadili, J., Aubert, G., Revenu, M., Saloux, E.: Region-based Active Contour with Noise and Shape Priors. In: Proc. of Int. Conf. on Image Processing (ICIP), pp. 1649–1652 (2006)
- [9] Narayanan V.M, Shankar P. M. , Reid J.M.: Non-Rayleigh statistics of ultrasonic back scattered signals. IEEE Trans. Ultrason., Ferroelect., Freq., Contr., vol. 41, no. 6, pp. 845-852. IEEE (1994)
- [10] Noble, J.A., Boukerroui, D.: Ultrasound Image Segmentation: A Survey. IEEE Transactions on Medical Imaging 25, pp. 987–1010 (2006)
- [11] Noble, J.A.: Ultrasound image segmentation and tissue characterization. In: Proceedings of the Institution of Mechanical Engineers, Part H: Journal of Engineering in Medicine 224, 2 (2010), 307.
- [12] Perreault, C., Auclair-Fortier, M.F.: Speckle Simulation Based on B-Mode Echographic Image Acquisition Model. In: Proc. of Can. Conf. on Computer and Robot Vision (CRV), pp. 379–386 (2007)
- [13] Reichl, T., Passenger J., Acosta O., Salvado O.: Ultrasound goes GPU: real-time simulation using CUDA. In: Proc. of SPIE (2009)
- [14] Sawatzky, A., Tenbrinck, D., Jiang, X., Burger, M.: A Variational Framework for Region-Based Segmentation Incorporating Physical Noise Models. Journal of Mathematical Imaging and Vision 47(3), pp. 179–209 (2013)
- [15] Segars, W.P., Sturgeon, G., Mendonca, S., Grimes, J., Tsui, B.M.W.: 4D XCAT Phantom for Multimodality Imaging Research. Med. Phys. 37(9), pp. 4902–4915 (2010)
- [16] Shankar P. M.: A General Statistical Model for Ultrasonic Backscattering from Tissues. IEEE Trans. Ultrason., Ferroelect., Freq., Contr., vol. 47, no. 3, pp. 727-736. IEEE (2000)
- [17] Tenbrinck, D., Schmid, S., Jiang, X., Schäfers, K., Stypmann, J.: Histogram-Based Optical Flow for Motion Estimation in Ultrasound Imaging. JMIV 47(1), pp. 138–150 (2013)
- [18] Tenbrinck, D., Sawatzky, A., Jiang, X., Burger, M., Haffner, W., Willems, P., Paul, M., Stypmann, J.: Impact of Physical Noise Modeling on Image Segmentation in Echocardiography. In: Proc. of Eurographics Workshop on Visual Computing for Biomedicine (VCBM), pp. 33–40 (2012)
- [19] Vorländer M.: Auralization: Fundamentals of Acoustics, Modeling, Simulation, Algorithms and Acoustic Virtual Reality. Springer (Berlin. Print). (2008)
- [20] Wein, W., Khamene, A., Clevert, D.-A., Kutter, O., Navab, N.: Simulation and Fully Automatic Multimodal Registration of Medical Ultrasound. In: Proc. of Int. Conf. on Medical Image Computing and Computer Assisted Intervention (MICCAI), pp. 136-143 (2007)
- [21] Zhu, Y., Magee, D., Ratnalingam, R., Kessel, D.: A virtual ultrasound imaging system for the simulation of ultrasound-guided needle insertion procedures. In: Proc. of Medical Image Understanding and Analysis (2006).